ELSEVIER

Physica C 304 (1998) 245–254

PHYSICA C

Formation of secondary phases in $YBa_2Cu_3O_{7-\delta}/SrTiO_3$ multilayers

C.N.L. Edvardsson [a,*,1], U. Helmersson [a], L.D. Madsen [a], Zs. Czigany [b], L. Ryen [c], E. Olsson [c,2]

[a] *Department of Physics, Linköping University, SE-581 83 Linköping, Sweden*
[b] *Research Institute for Technical Physics, P.O. Box 76, H-1325 Budapest, Hungary*
[c] *Department of Physics, Chalmers University of Technology, SE-412 96 Göteborg, Sweden*

Received 6 April 1998; revised 11 June 1998; accepted 18 June 1998

Abstract

The $YBa_2Cu_3O_{7-\delta}$ (YBCO)/$SrTiO_3$ (STO) material system has a potential for device applications such as superconducting field effect transistors, filters and delay lines, due to the possibility to grow heteroepitaxial structures with the necessary orientation of the highly anisotropic superconductor YBCO. To investigate microstructure and formation of secondary phases in this material system, YBCO/STO multilayers were grown by DC and rf magnetron sputtering, respectively. The formation of a previously unidentified cubic (or pseudo-cubic) phase with a lattice parameter of 0.414 nm, containing Ba, Ti, O, and Y, is reported. It is suggested that this phase is Y-substituted $BaTiO_3$ (BTO), with Y in both the Ba and Ti positions of the perovskite unit cell. This new phase was observed to predominantly nucleate on the substrate surface and to be embedded in the layered structure. The precipitates were found to have a cube-on-cube orientational relationship to the $LaAlO_3$ (LAO) substrate, as well as to the STO and YBCO layers. Y_2O_3 inclusions were also found in the multilayers.

PACS: 74.76; 77.55

Keywords: Phase formation; Multilayered structures; Magnetron sputtering

1. Introduction

Heteroepitaxial multilayered structures of high-T_c superconductors (HTSs) and insulators exhibit a large potential to be used in applications such as superconductor–insulator–superconductor (SIS) Josephson junctions, transmission line devices, and three-terminal devices. Such applications require a high critical current density ($> 10^6$ Å/cm^2) of the HTS, achieved in heteroepitaxial structures by the induced orientation of the highly anisotropic HTS. Another requirement on such structures are sharp transitions from the superconductor to the insulator implying an absence of interface reactions during growth and subsequent processing. The insulator layers of course have

* Corresponding author. Tel.: +46-1328-1257; Fax: +46-1313-7568; E-mail: nic@ifm.liu.se

[1] Previously C.N.L. Johnson.

[2] Present address: The Ångström Laboratory, Uppsala University, SE-751 21 Uppsala, Sweden.

0921-4534/98/$ - see front matter
PII: S0921-4534(98)00310-4

to be continuous to avoid short circuits. During growth of structurally complicated oxides also the precipitation of secondary phases should be avoided, since they most probably will affect the properties of the structures in a negative sense, except when the small precipitates in the HTS layers act as flux pinning centers.

The formation of stable and meta-stable secondary phases, such as Y_2O_3 (yttria) precipitates in $YBa_2Cu_3O_{7-\delta}$ (YBCO) [1] or the pyrochlore phase ($A_2B_2O_7$) appearing in lead-based perovskite (ABO_3) ferroelectrics [2], is a commonly observed phenomenon in growth of complex oxides. In general the complex oxides are less stable than simpler oxides and since they contain a larger number of elements, several different secondary phases can form. Furthermore, the often used physical vapor deposition techniques, magnetron sputtering and laser ablation, are far from equilibrium processes, which leads to kinetic limitations such as limited surface migration also influencing phase formation.

Most of the superconductor–insulator multilayers studied so far consist of YBCO as the HTS layer and CeO_2 [3], $SrTiO_3$ (STO) [4] and $PrBa_2Cu_3O_7$ [5–7] as the insulating layer. In the present study the high dielectric material STO was combined with YBCO. The high and tunable dielectric constant as well as the relatively moderate lattice and thermal expansion mismatch has made STO the most studied insulator in combination with YBCO in field-effect experiments [8–10].

When growing YBCO/STO multilayered structures the Sr and Ti cations from STO imposes an additional complexity to the overall metal oxide phase diagram. Already the $YO_{1,5}$–BaO–CuO phase diagram contains about 10 stable phases at commonly used deposition conditions. The copper oxide (CuO_x) surface particles often reported on single YBCO thin films [11–14] are one of the stable secondary phases in the phase diagram. It is crucial to avoid the formation of such surface particles due to their large size and density when growing multilayered structures. We have previously shown [15] that the CuO_x surface particle formation can be significantly reduced by using N_2O in the process gas in combination with Y-rich sputtering targets. To facilitate the growth of YBCO/STO multilayers, a sputtering process was developed for STO with the aim of optimizing growth of epitaxial, single crystal films at YBCO processing parameters [16].

Four multilayers were analyzed in this study. Structural and chemical characterization were made by X-ray diffraction (XRD), high-resolution transmission electron microscopy (HRTEM), energy-dispersive X-ray spectroscopy (EDS), and electron energy-loss spectroscopy (EELS). All four multilayers were investigated using XRD and two of them were selected for cross-sectional HRTEM, EDS and EELS analysis.

The results show that YBCO/STO multilayers with sharp interfaces can be grown, but that precipitation of secondary phases is a problem at the growth conditions used. One of the phases formed is a previously unidentified cubic (or pseudo-cubic) phase with a lattice parameter of 0.414 nm, containing Ba, Ti, O, and Y. This phase is suggested to be Y-substituted $BaTiO_3$ (BTO), with Y in both the Ba and Ti positions of the perovskite unit cell. The $(Ba_{1-x},Y_x)(Ti_{1-x},Y_x)O_3$ perovskite was pre-dominantly observed to nucleate on the substrate surface. Small yttria inclusions also formed in the HTS layers.

2. Experimental

The YBCO and STO films were grown using DC and rf magnetron sputtering, respectively. Both sputtering targets were ceramic disks 50 mm in diameter and 5 mm thick. The YBCO target had a 30% excess of Y [15], while the STO target was stoichiometric [16]. An off-axis geometry, with the targets facing each other with their common normal at an angle of 90° to the substrate normal, was used to avoid energetic bombardment of the growing films. The magnetrons were configured to have repelling magnetic fields. Target shutter movements were controlled by a computer via an electric–pneumatic interface to obtain the desired periodic structure. To achieve stable sputtering conditions the targets were presputtered with target and substrate shutters closed for 60 and 15 min for YBCO and STO, respectively. A total output rf power of 80 W was used for sputtering of the STO, and a DC current of 400 mA (resulting in a target voltage of 130 V) was used for the YBCO deposition. The depositions were made in

a high-vacuum system with a base pressure of 3.3×10^{-5} Pa (2.5×10^{-7} Torr) which has been described in detail elsewhere [1]. Polished $(001)_c$ pseudo-cubic $LaAlO_3$ (LAO) substrates, 10×10 mm^2 in size were affixed with silver paste to a substrate holder block maintained at a temperature of 740°C during the deposition process. The total sputtering pressure was maintained at 14.4 Pa (108 mTorr) as measured by a capacitance manometer. A control unit regulating the gas flows proportionally was used to ensure a constant $Ar:O_2:N_2O$ gas composition of 3:1:0.13. The purity of the gases were 99.998% for both Ar and O_2 and 99.995% for N_2O.

The multilayers were grown to a total thickness of approximately 200 nm corresponding to 22–30 STO/YBCO bilayers. STO was always deposited as the first layer. The same post-deposition oxygen annealing sequence as for single YBCO films was used for the multilayers. First, the temperature was rapidly decreased from the growth temperature to approximately 600°C, pure oxygen was then introduced to a pressure of 0.5 atm followed by a slow cool-down (4°C/min) to approximately 150°C and finally the chamber was vented with dry nitrogen.

Structural and chemical characterization were made by XRD, HRTEM with selected area electron diffraction (SAED), EDS, and EELS. In the XRD analyses, both a Bragg–Brentano Θ–2Θ geometry (Philips PW 1820 powder diffractometer) and a four-circle geometry (Philips MRD) were used. The Bragg–Brentano Θ–2Θ geometry was utilized to determine the crystalline phases present in the film and the four-circle geometry was used to obtain reciprocal space maps (RSMs) in order to determine orientation relationships. In both cases, Cu K_α radiation was used and the optics utilized on the powder diffractometer were a Ni β-filter and a $1/2°$ divergence slit on the primary side and a $1/2°$ receiving slit and a curved graphite secondary monochromator on the secondary side. The MRD system was equipped with a Ni β-filter and a 1×1 mm^2 collimator slit on the primary side and parallel plate collimator and a flat graphite secondary monochromator on the secondary side. The structural characteristics of the multilayers were also studied by TEM. Cross-sectional TEM specimens were prepared by placing two slices of the samples glued together film-to-film into a window in a Ti disc [17]. The thin discs were then ground mechanically to a thickness of 50 μm followed by polishing with a 1-μm diamond polishing paste. Finally, the discs were thinned to electron transparency by ion beam milling. An angle of 4° with respect to the milled surface was used. The ion milling was completed with 3 min of ion beam polishing at a voltage of 3 kV. HRTEM and EDS was carried out in a Philips CM 20 UT microscope using an accelerating voltage of 200 kV and the SAED was performed in a JEOL 2000 FX also at 200 kV. EELS characterization was performed in a Philips CM 200 Super Twin field emission gun microscope with a Gatan Imaging Filter (GIF), which was used for elemental mapping. The electron energies used for the elemental mapping were Ba M_5 (781 eV), Ti L_3 (456 eV), Cu L_3 (931 eV) and Y L_3 (2080 eV).

Bulk oxide samples with the cation compositions (Ba:Y:Ti) 4:4:0, 4:3:1, 4:2:2, 4:1:3 were prepared for comparative XRD analysis. These samples were obtained by sintering powders of $BaCO_3$, Y_2O_3 and TiO_2. The powders were first mixed and calcinated at 1000°C then ground and pressed and finally sintered at 1200°C.

3. Results

Table 1 summarizes the samples studied with respect to their nominal layer thicknesses. Also the layer periodicity values measured are given in Table 1. All four multilayers (A–D) grown in this study were investigated using XRD. The samples A and B were also selected for cross-sectional HRTEM analysis.

The YBCO layers in all samples were *c*-axis oriented, i.e., the *c*-axis was perpendicular to the substrate surface. Hence, only the 00ℓ reflections of YBCO could be detected in Θ–2Θ diffractograms, as shown in Fig. 1. The *c*-axis was calculated, using the 005 reflection, to be 1.169 nm for all samples. Also the STO layers grew epitaxially resulting in an overlap between the 001 and the 002 reflections of STO with the 003 and 006 reflections of YBCO, respectively. The overlap was manifested in the diffractograms by a higher intensity (as compared to standards [18]) of these two peaks in relation to the other YBCO 00ℓ peaks. A shift in the peak posi-

Table 1
Multilayers investigated in this study

Sample	Nominal YBCO thickness (nm)	Nominal STO thickness (nm)	Nominal multilayer period (nm)	Measured multilayer period (nm)
A	7.4	1.9	9.3	9.3
B	5.0	2.9	7.9	7.7
C	3.7	3.8	7.5	7.5
D	3.5	3.5	7.0	6.8

Nominal layer thicknesses, nominal multilayer period and multilayer period as measured by low angle XRD are given.

tions of these two peaks depending on the ratio between the individual YBCO and STO layer thicknesses was also observed. Although the YBCO layers were enclosed between STO layers, the YBCO *c*-axis length was the same as for superconducting single-layer YBCO films indicating that the standard post-deposition oxidization process used was sufficient to fully oxidize the YBCO layers. The layered structure and the *c*-axis orientation of the YBCO constrains the main oxygen diffusion path to be in the basal plane of the unit cell. A sufficient oxidization is nevertheless to be expected, since it has been shown that the diffusion in the basal plane is 10^4–10^6 times faster than along the *c*-axis [19]. In addition to reflections originating from YBCO, STO, and LAO (substrate) a few other reflections were also observed in the diffractogram shown in Fig. 1. A 004 reflection from yttria at $2\Theta = 33.97°$ (0.264 nm) and two reflections, not readily identified, at $2\Theta = 21.53°$ (0.413 nm) and $2\Theta = 43.74°$ (0.207 nm), respectively, can be seen. Since one of the two latter reflections is a multiple of the other, it is assumed that they both originate from the same secondary phase. The intensity of these three impurity reflections was found to increase with increasing YBCO layer thicknesses.

XRD analysis was also used to determine the multilayer period by recording the low angle ($0.9° \leq 2\Theta \leq 5.0°$) reflections originating from the multilayer periodicity. The Θ–2Θ diffractograms showed only two peaks caused by the periodicity of the layered structure. Such a diffractogram from sample B, is shown in Fig. 2. The widths of the reflections indicate a low number of periods (22) and inhomogeneous layer thicknesses. A $\sin^2\Theta$–n^2 linearization of the modified Bragg's law [20,21] was used to determine the period when two peaks could be resolved. The calculated period from the diffractogram in Fig. 2 was 7.7 nm and the corresponding calcula-

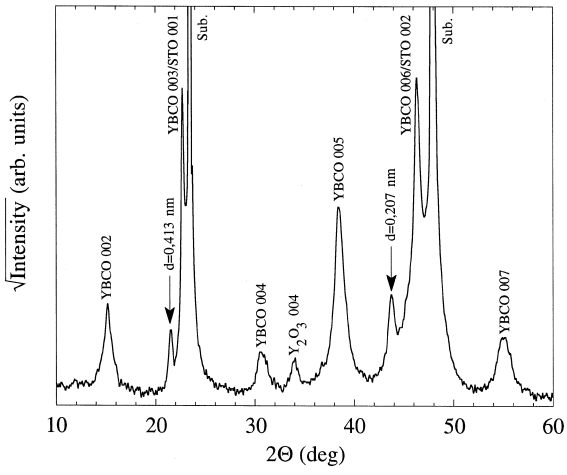

Fig. 1. Overview Θ–2Θ diffractogram of a YBCO/STO multilayer (sample A) showing the YBCO 00ℓ, STO 00ℓ (overlapping with YBCO), Y_2O_3 004, substrate and unidentified phase reflections. The reflections of the unidentified phase are indicated by arrows and the corresponding lattice spacings are given.

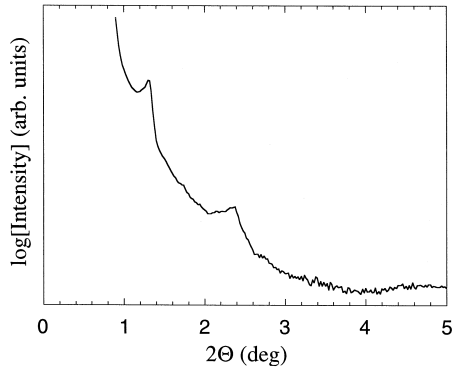

Fig. 2. Low angle Θ–2Θ diffractogram of sample B showing two peaks caused by the periodicity of the layered structure.

tion on sample A was found to be in accordance with the nominal value 9.3 nm (see Table 1).

The samples A and B were also characterized by TEM. This analysis showed distinct layers and sharp but slightly wavy interfaces between the YBCO and STO layers, as shown in the cross-sectional TEM micrograph from sample A in Fig. 3. The layer thicknesses for both YBCO and STO vary in each individual layer and also between separate layers. The average thickness of the STO and YBCO layers in this sample, with a multilayer period of 9.3 nm (XRD-value) was measured from the micrograph in Fig. 3 to be 2.9 and 6.8 nm, respectively. The lattice parameter of the LAO substrate (0.3792 nm) was used to calibrate the thickness measurements. The STO layers appear to be free of major defects whereas, the YBCO layers contain stacking faults and subgrain boundaries. Yttria inclusions were identified by comparing lattice fringe spacings with literature values and interplanar spacings obtained from the XRD measurements. Furthermore, lattice fringes from an additional phase were observed with fringe spacings corresponding to a lattice spacing of 0.414 nm, i.e., corresponding to the value obtained for the XRD peak at $2\Theta = 21.53°$ (0.413 nm). Fig. 4 (from sample A) shows a HRTEM micrograph in which both kinds of inclusions are visible.

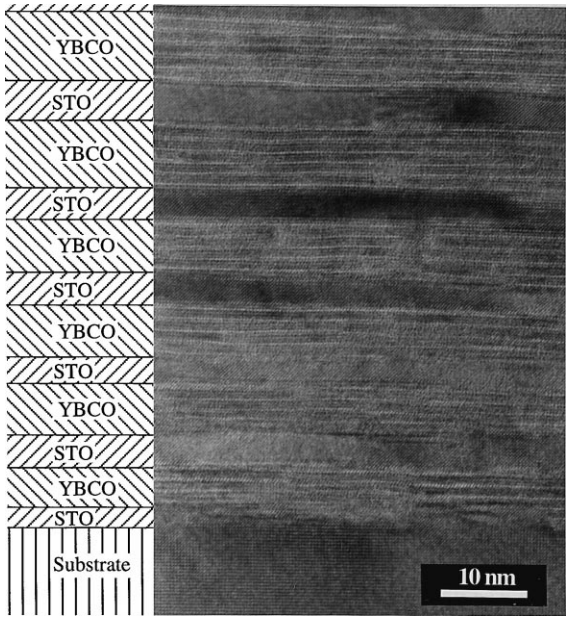

Fig. 3. Cross-sectional TEM micrograph of sample A.

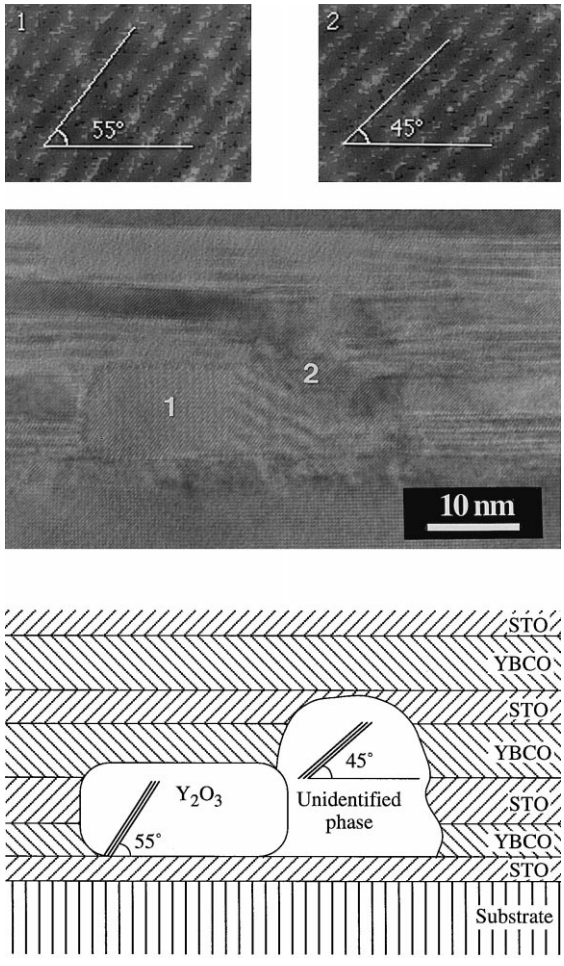

Fig. 4. Cross-sectional TEM micrograph from sample A and explanatory schematic showing on the left hand side an yttria inclusion with resolved (111) planes that has nucleated on the first deposited STO layer. To the right of the yttria inclusion, partly superposed, there is an inclusion of the unidentified phase. The two pictures on top are magnifications of the areas indicated by numbers in the micrograph.

The planes from YBCO, STO, and Y_2O_3 resolved in Fig. 4 show that the orientation relationships can be described as: $(001)_{STO}\|(001)_{Y_2O_3}\|(001)_{YBCO}$ with $[100]_{STO}\|[110]_{Y_2O_3}\|[100]_{YBCO}$. The yttria inclusions thus exhibit an azimuthal 45° rotated cube-on-cube orientation to both YBCO and STO. Their orientation is the same as reported earlier [1,11,22,23]. The yttria inclusions were also observed to nucleate on

both STO and YBCO layers, with a cross-sectional size of 20–30 nm laterally and 11–13 nm in height.

The inclusions of the unidentified phase were found to be approximately 40×40 nm^2 in cross-section. They had predominantly nucleated on the LAO substrate and were embedded in the layered structure, as shown in Fig. 5 from sample A, but could also be identified further into the films next to yttria inclusions. The existence of misfit dislocations in the interface between the inclusion and LAO substrate was also established as indicated in Fig. 5. The lattice spacings obtained from electron diffraction were 0.414 nm perpendicular to the substrate surface, 0.417 nm in the plane parallel to the surface and 0.294 nm at an angle of 45° to the surface. The diffraction spots of the LAO substrate were used to calibrate the measurements in the SAED patterns. As a comparison to the lattice spacings and directions

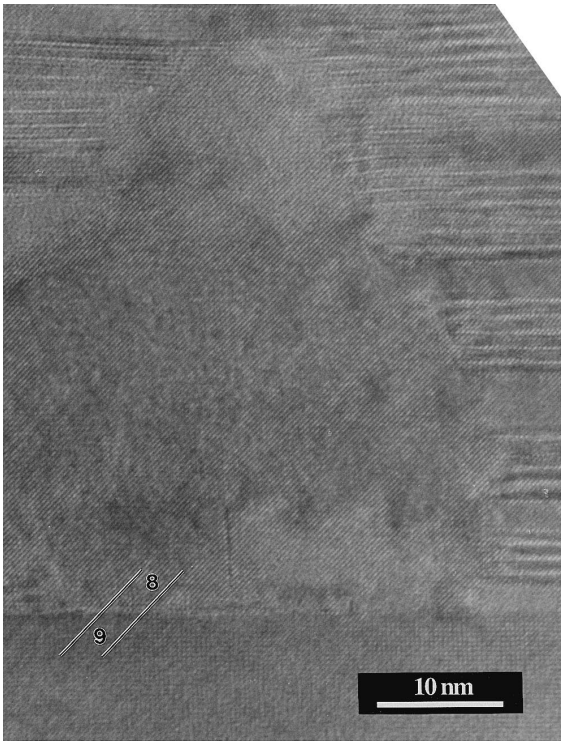

Fig. 5. Cross-sectional TEM micrograph from sample A showing part of an inclusion of the unidentified phase that has nucleated on the substrate surface and is embedded in the layered structure. The presence of misfit dislocations in the inclusion–substrate interface is shown by the number of lattice planes between the two parallel lines.

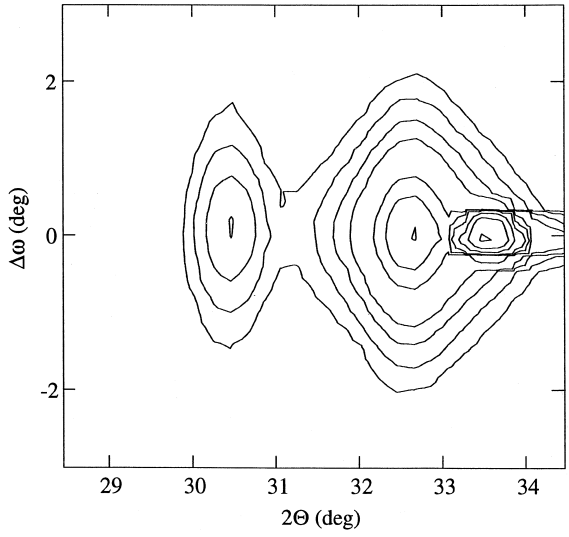

Fig. 6. RSM from sample A of the region containing the overlapping STO 011, YBCO 013, and YBCO 103 reflections.

found by SAED the same kind of information was obtained by XRD mapping of the STO 011 and 111 reflections. The RSM from sample A in Fig. 6 shows three reflections; a broad reflection at a 2Θ angle of 30.41° (0.294 nm), the overlapping STO 011, YBCO 013 and YBCO 103 reflections at 32.60° (0.275 nm) and the LAO 011_c reflection at 33.45° (0.268 nm). Analogously, also a weak reflection at 37.34° (0.241 nm) could be detected in the same RSM as the overlapping STO 111 and YBCO 113 reflections (not shown).

To analyze the chemical composition of the unidentified phase, an EDS spectrum was taken from such an inclusion in the cross-section sample. A clear reduction of the Sr and Cu signals was ob-

Table 2
EDS intensity of different peaks of the layered structure and an inclusion of the unidentified phase

Peak	Layered structure	Inclusion
Y (K_α)	121	99
Ba (L_α) + Ti (K_α)	697	735
Cu (K_α)	547	177
Sr (K_α)	67	29

For comparison the intensities of the inclusion measurement have been normalized to the intensity of the O (K_α) peak.

served in comparison to a spectrum from the layered structure, but due to the overlap between Ba L_α, L_β, and Ti K_α, K_β, respectively, it could not be ascertained from EDS whether Ti was present or not. The EDS peak intensities from an inclusion of the unidentified phase and from the layered structure are shown in Table 2. Elemental mapping was also carried using EELS and these results clearly showed the presence of Ti in the inclusions, as can be seen in Fig. 7 which shows EELS elemental maps of the inclusion. Also the presence of Ba and the absence of Cu (not shown) was verified in the EELS analysis. Although it was difficult to detect both Y and Sr with this method, the results indicate the presence of Y in the inclusions.

Bulk samples of four different compositions were made by a standard sintering technique to investigate the phase formation in the Ba–Y–Ti–O system closer to thermal equilibrium. XRD Θ–2Θ scans of these bulk samples showed no existence of the unidentified phase, i.e., none of the earlier reflections found could be detected in any of the sintered samples. In the Ba–Y–O sample mainly $Ba_3Y_4O_9$ reflections were detected together with some weak Y_2O_3 reflec-

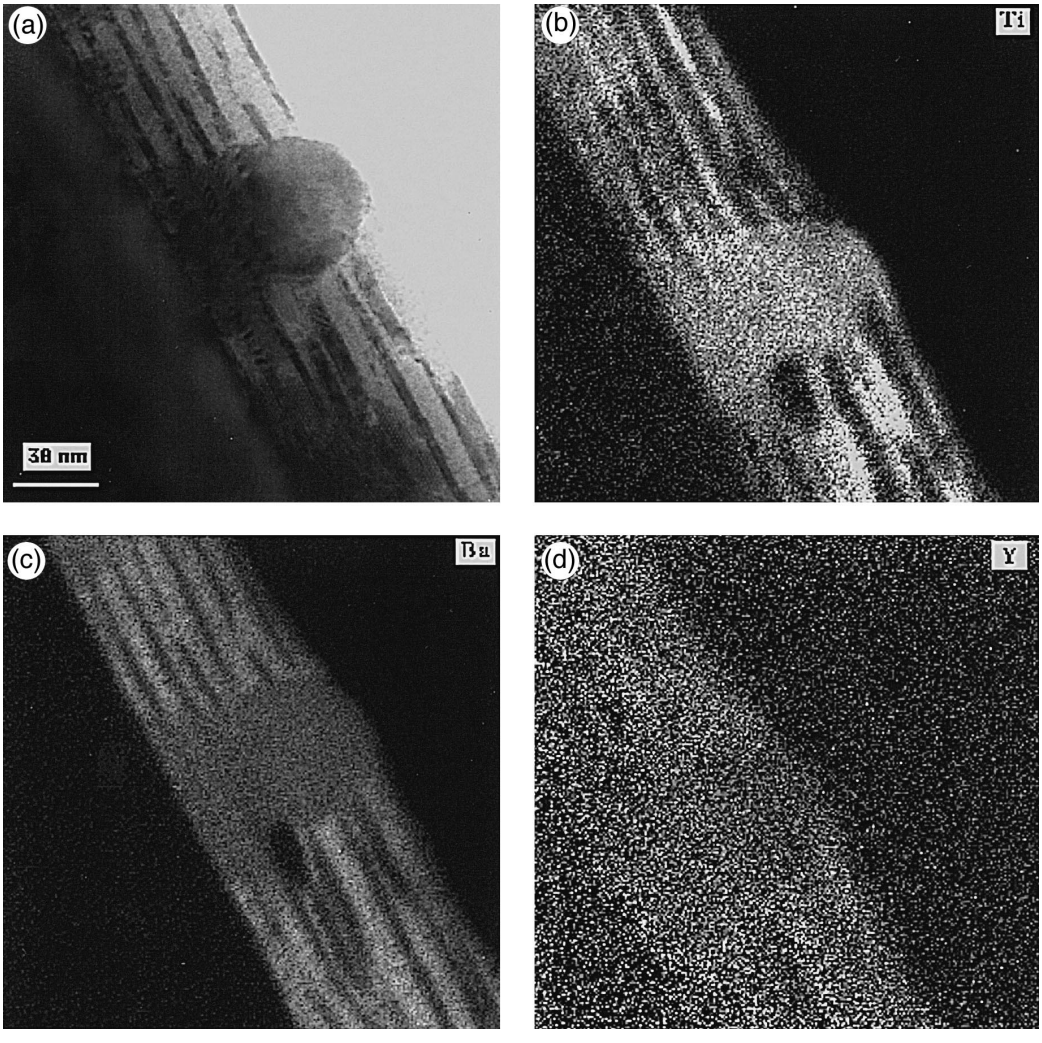

Fig. 7. Elemental distribution maps obtained by energy-loss filtered imaging showing: (a) conventional image, (b) Ti distribution, (c) Ba distribution, and (d) Y distribution.

tions. As the Ti content was increased at the expense of the Y content also BTO reflections appeared.

4. Discussion

YBCO/STO multilayers have been grown without any formation of large CuO_x particles. The half-sphere shaped CuO_x surface particles can have a diameter of 200–250 nm on only 10 nm thick YBCO films [24], and if present they will severely disturb the growth and properties of layered structures. Precipitation of yttria inclusions and of an unidentified phase was, however, not avoided. The presence of yttria inclusions is not surprising since it has been observed many times in YBCO films [1,11,22,23,25], especially at deposition conditions with Y-rich sputtering targets [15]. Yttria inclusions will not cause any short circuits, since yttria is an insulator. Furthermore, deterioration of the transport properties of the superconducting layers is not expected since the inclusions are relatively small and in fact they can be beneficial in terms of flux pinning centers. On the other hand, the appearance of the unidentified phase was unexpected. STO has been widely used as a substrate for thin film depositions of YBCO without any formation of secondary phases at the substrate temperature used in the present study. Reactions between STO substrates and YBCO thin films have been found at substrate temperatures above 850°C [26] and in solid state diffusion reactions, by firing mixtures of STO and YBCO powders, formation of secondary phases has been observed only above 950°C [26].

The two reflections of the unidentified phase found in the RSMs could be indexed as the 011 (Fig. 6) and 111 reflections of a cubic crystal with a lattice parameter of 0.414 nm, which is the plane spacing that was found perpendicular to the film surface. The indices are based on the definition of the normal of the film surface as the [001] direction. Hence, the unidentified phase is cubic (or pseudo-cubic) and oriented in the same manner as LAO, STO and YBCO (cube-on-cube). The XRD and SAED lattice spacing measurements show a good correspondence; the (001) spacing is measured to 0.413 and 0.414 nm in XRD and SAED, respectively, and the (011) spacing to 0.294 nm with both methods.

The chemical characterization of the unidentified phase by EELS elemental mapping clearly showed the presence of Ba and Ti. EDS also showed the presence of Ba. The difficulty to confine the electron beam only to the inclusion due to the small inclusion size, is probably the reason that all examined elements could be detected to some extent in the EDS analysis. However, the reduction of the Y signal, as compared to the reductions of the Sr and Cu signals, is interpreted as an indication of Y being present and Sr and Cu being absent. The absence of Cu was also verified by EELS. The weak signal in the Y-map (Fig. 7d) is a result of using the only available high energy-loss peak (Y L_3 at 2080 eV). Nevertheless, the EELS analysis also indicates that Y is present in the inclusions.

In summary, the unidentified phase found was cubic (or pseudo-cubic), with a lattice parameter of 0.414 nm, containing Ba, Ti, O, and Y. The orientation is the same as of the other compounds in the structure, i.e., cube-on-cube.

To our knowledge there is no reported cubic (or pseudo-cubic) barium titanium yttrium oxide with a lattice constant of 0.414 nm or a multiple of 0.414 nm. The JCPDS Powder Diffraction Files (Sets 1–46) and the NIST Crystal Data (Vol. CDF-95H) have been searched. Derks et al. [26] have reported on the formation of $YBa_3Ti_2O_{8,5}$ at 950°C in YBCO/STO powder mixtures heated in air, but $YBa_3Ti_2O_{8,5}$ is hexagonal and has no interplanar spacings that coincides with the results found. Lattice constants of $\approx 0{,}4$ nm or multiples thereof are common for the perovskites (ABO_3) and spinels (A_2BO_4), since the dominating factor that determines the lattice constants of these structures is the close-packing of oxygen ($-$II) ions. The chemical characterization of the unidentified phase indicates that the perovskite BTO is a possible candidate, but the lattice constant of BTO is only 0.403 nm. However, prolongation of the *c*-axis to 0.420 nm has been reported [27,28] for tetragonal BTO in thin films of approximately 10 nm thickness. The cause of the prolonged *c*-axes was found to be strain due to the stress created in the interface to the Pt(100)/MgO(100) substrates. Since the inclusions found have in-plane and out-of-plane lattice parameters roughly the same, and misfit dislocations are observed in the inclusion–substrate interface (Fig. 5) as a consequence of stress relief, an

unstrained lattice seems likely. However, a small content of Y, which was indicated to be the case, could cause an enlargement of the BTO unit cell since the Y ion is larger than the Ti ion. The A and B cations in perovskites must have a total valence of +VI to balance the −VI of the oxygen anions. Furthermore as a geometrical constraint, the B cation must be small enough to fit in the octahedral positions of the oxygen sublattice. Considering the possibility of a $(Ba_{1-x},Y_x)(Ti_{1-x},Y_x)O_3$ perovskite, it is clear that the valence balance is fulfilled, but to place Y in the Ti positions requires some distortion of the oxygen sublattice. The partial substitution of the smaller Y ions in the Ba positions could allow such distortions of the O anion positions. It is assumed that the post deposition oxygen anneal fully oxidizes the perovskite structure. A x-value of 0.01–0.02 is found treating the ions as hard spheres and by assuming a linear increase of ionic radius with composition (Vegard's law).

Although only a few compositions were used in the sintered bulk samples, the fact that no signs of the unidentified phase could be detected indicates that the formation is caused by kinetic limitations. A reduced surface mobility has been observed, when using N_2O in the sputtering gas [15]. Phase formation could also be influenced by a non-stoichiometric composition on the growth surface. Earlier it was found that STO films grown under similar conditions were Sr-deficient, but still contained only one phase [29].

5. Summary

An unidentified phase cubic (or pseudo-cubic) with a lattice parameter of 0.414 nm containing Ba, Ti, O, and Y was found when growing YBCO/STO multilayers by means of DC and rf sputtering. This phase is suggested to be Y-substituted $BaTiO_3$, with Y in both the Ba and Ti positions of the perovskite unit cell. The $(Ba_{1-x},Y_x)(Ti_{1-x},Y_x)O_3$ perovskite was observed to predominately nucleate on the substrate surface and to be embedded in the layered structure. It has a cube-on-cube orientational relationship to the LAO substrate, STO and YBCO. Yttria inclusions also formed in the multilayers. Finally, it was noticed that the oxidization of YBCO in the layered structure, with the same post-deposition anneal as used for single YBCO film growth, appeared to be sufficient, based on the length of the YBCO c-axis as measured by XRD.

Acknowledgements

This work was carried out with the financial support of the Swedish Thin Film and Superconductor Consortia. G. Radnoczi, B. Pécz, M.P. Johansson, and L. Hultman are gratefully acknowledged for their valuable help with TEM operation and evaluation. Discussions with J.-E. Sundgren, X. Wang, S.N. Jacobsen and experimental assistance from L.-D. Wernlund, K. Brolin and T. Lingefelt are also highly appreciated.

References

[1] T.I. Selinder, U. Helmersson, Z. Han, L.R. Wallenberg, Thin Solid Films 229 (1993) 237.
[2] H.-F. Cheng, J. Appl. Phys. 78 (1995) 4633.
[3] M.W. Denhoff, P.D. Grant, J.P. McCaffrey, Can. J. Phys. 70 (1992) 1124.
[4] J.P. Contour, D. Ravelosona, C. Sant, C. Frétigny, C. Dolin, J. Rioux, P. Auvray, J. Caulet, J. Cryst. Growth 141 (1994) 141.
[5] S.J. Pennycook, M.F. Chisholm, D.E. Jesson, D.P. Norton, D.H. Lowndes, R. Feenstra, H.R. Kerchner, J.O. Thomson, Phys. Rev. B 67 (1991) 765.
[6] J.D. Budai, M.F. Chisholm, R. Feenstra, D.H. Lowndes, D.P. Norton, L.A. Boatner, D.K. Christen, Appl. Phys. Lett. 58 (1991) 2174.
[7] P. Lerch, F. Marcenat, P. Jacot, D. Ariosa, J. Perret, C. Leemann, P. Martinoli, M. Cantoni, H.R. Ott, Physica C 242 (1995) 30.
[8] K. Joosse, Y.M. Boguslavskij, G.J. Gerritsma, H. Rogalla, Physica C 224 (1994) 179.
[9] J. Mannhart, J.G. Bednorz, K.A. Müller, D.G. Schlom, Z. Phys. B 83 (1990) 307.
[10] C.M. Jackson, J.H. Kobayashi, A.Z. Kain, A. Lee, C. Pettiette-Hall, J.F. Burch, R. Hu, R. Hilton, Integrated Ferroelectrics 4 (1994) 121.
[11] T.I. Selinder, U. Helmersson, Z. Han, J.-E. Sundgren, H. Sjöström, L.R. Wallenberg, Physica C 202 (1992) 69.
[12] C.C. Chang, X.D. Wu, R. Ramesh, X.X. Xi, T.S. Ravi, T. Venkatesan, D.M. Hwang, R.E. Muenchausen, S. Foltyn, N.S. Nogar, Appl. Phys. Lett. 57 (1990) 1814.
[13] V. Matijasevic, P. Rosenthal, K. Shinohara, A.F. Marshall, R.H. Hammond, M.R. Beasley, J. Mater. Res. 6 (1991) 682.

[14] Y.Q. Li, J. Zhao, C.S. Chern, P. Lu, B. Gallois, P. Norris, B. Kear, F. Cosandey, Physica C 195 (1992) 161.
[15] C.N.L. Johnson, U. Helmerson, L.D. Madsen, S. Rudner, L.-D. Wernlund, J. Appl. Phys. 77 (1995) 6388.
[16] L.D. Madsen, C.N.L. Johnson, S.N. Jacobsen, U. Helmersson, S. Rudner, I. Ivanov, L.-D. Wernlund, L. Ryen, E. Olsson, Microelectron. Eng. 29 (1995) 123.
[17] A. Barna, Topographic kinetics and practise of low angle ion beam thinning, in: R. Anderson, B. Tracy, J. Braman, (Eds.), Mat. Res. Soc. Proc., MRS, Pittsburg, 254 (1991) 3.
[18] Joint Committee of Powder Diffraction Standards—JCPDS file no. 40–159, International Centre for Diffraction Data, Newtown Square, USA.
[19] S.J. Rothman, J.L. Routbort, U. Welp, J.E. Baker, Phys. Rev. B 44 (1991) 2326.
[20] B.K. Agarwal, X-ray Spectroscopy—An Introduction, 1st edn., Springer-Verlag, Berlin, 1979, p. 135.
[21] V. Dupuis, M.F. Ravet, C. Tête, M. Piecuch, B. Vidal, J. Appl. Phys. 68 (1990) 3348.
[22] A. Catana, R.F. Broom, J.G. Bednorz, J. Mannhart, D.G. Schlom, Appl. Phys. Lett. 60 (1992) 1016.
[23] P. Lu, Y.Q. Li, J. Zhao, C.S. Chern, B. Gallois, P. Norris, B. Kear, F. Cosandey, Appl. Phys. Lett. 60 (1992) 1265.
[24] Z. Han, T.I. Selinder, U. Helmersson, J. Appl. Phys. 75 (1994) 2020.
[25] B. Schulte, M. Maul, P. Häussler, W. Becker, M. Schmelz, M. Steins, H. Adrian, J. Alloy Compounds 195 (1993) 299.
[26] W.P.T. Derks, H.A.M.V. Hal, C. Langereis, Physica C 156 (1988) 62.
[27] Y. Yano, K. Iijima, Y. Daitoh, T. Terashima, Y. Bando, Y. Watanabe, H. Kasatani, H. Terauchi, J. Appl. Phys. 76 (1994) 7833.
[28] Y. Yoneda, H. Kasatani, H. Terauchi, Y. Yano, T. Terashima, Y. Bando, J. Cryst. Growth 150 (1995) 1090.
[29] L. Ryen, E. Olsson, L.D. Madsen, X. Wang, C.N.L. Edvardsson, S.N. Jacobsen, U. Helmersson, S. Rudner, L.-D. Wernlund, J. Appl. Phys., 1998, accepted for publication.